ChemPubSoc Europe

DOI: 10.1002/celc.201600178

CHEMELECTROCHEM Articles

A Hydrogen-Bonded Organic-Framework-Derived Mesoporous N-Doped Carbon for Efficient Electroreduction of Oxygen

Ji Liu,[a] Ligui Li,*[a, b] Wenhan Niu,[a] Nan Wang,[a] Dengke Zhao,[a] Shuaibo Zeng,[a] and Shaowei Chen[a, c]

Direct carbonization methods represent a facile strategy for the synthesis of functional carbon electrocatalysts, however, the resulting carbons are mostly microporous and of low surface area, which disfavor mass transfer, and usually have low electrocatalytic activity. In this study, a hydrogen-bonded organic framework (HOF) comprising of melamine and trimesic acid is used as a highly porous precursor to prepare N-doped carbons through facile, direct pyrolysis. The high nitrogen content of melamine and the intrinsically porous nature of the HOF facilitates the formation of a mesoporous carbon with 4.8 atom% content of nitrogen dopants and a significantly high surface area of 1321 $m^2 g^{-1}$. Electrochemical measurements show that the best sample, which was pyrolyzed at 800 °C (HOF-800), exhibited efficient catalytic activity for oxygen electroreduction in 0.1 M KOH aqueous solution. This catalyst exhibits a much more positive onset potential, higher diffusion-limited current density, higher electron-transfer number in the low overpotential region, higher stability, and stronger tolerance against methanol crossover than the state-of-the-art Pt/C catalysts. The results in this study suggest the potential of intrinsically porous HOFs for the development of highly efficient nonprecious-metal electrocatalysts.

1. Introduction

The oxygen reduction reaction (ORR), which proceeds along complicated reaction pathways and hence has sluggish electron-transfer kinetics, represents a critical reaction process at the cathode of polymer electrolyte membrane fuel cells (PEMFCs) and metal–air batteries. Highly active catalytic materials typically guide the ORR along the preferred 4 e^- pathway, boost the reaction rate and simultaneously lower the electrochemical overpotential, both of which help to fulfill the power requirements for practical application. Precious metals, predominantly Pt, and their alloys, have been the universal choice materials for ORR catalysts. However, the disadvantages of precious metal catalysts, such as their limited reserves on Earth, poor stability, weak tolerance to poisoning species and high cost, are difficult to overcome and hence are the main factors limiting their large-scale production for real applications. Consequently, developing affordable alternatives with acceptable catalytic activity and durability for the ORR has become one of the foremost topics in research into PEMFCs and metal–air batteries.

Emerging carbon-based nanomaterials that are co-doped with earth-abundant transition metals (e.g., Fe and Co) and heteroatoms (e.g., N, B, P, and S), are considered to be promising alternatives for overcoming the aforementioned intrinsic drawbacks of Pt-based metals for the ORR.[1–5] In addition to the content of active components, the surface area and corresponding pore structures largely determine the amount of accessible active sites and hence the catalytic activity of these carbon-based catalysts.[3,6,7] Within this context, it is necessary to maximize the effective surface area and pore dimensions, such that the transfer of correlated ORR species (e.g., OH^-, H^+, O_2, and H_2O) promotes improved ORR catalytic activity.

To generate hierarchical porous structures and increase surface areas, large numbers of sacrificial templates (normally SiO_2 and Al_2O_3 nanoparticles or their porous nanostructured materials)[6,8,9] are usually required to implant into carbon precursors, complicating the preparation procedure and hindering the mass production of porous carbon-based catalysts. Thus, it is extremely desirable to produce highly porous carbon through direct carbonization without the implantation of sacrificial templates from the point views of both scientific research and industry. However, the reported carbons prepared by direct carbonization are mostly microporous and of low surface area, which disfavor mass transfer and usually have low electrocata-

[a] J. Liu, Prof. Dr. L. Li, W. Niu, N. Wang, D. Zhao, S. Zeng, Prof. Dr. S. Chen
New Energy Research Institute
College of Environment and Energy
South China University of Technology
Guangzhou Higher Education Mega Center
Guangzhou 510006 (China)
E-mail: esguili@scut.edu.cn

[b] Prof. Dr. L. Li
Guangdong Provincial Key Laboratory of Atmospheric Environment and Pollution Control, College of Environment and Energy
South China University of Technology
Guangzhou 510006 (China)

[c] Prof. Dr. S. Chen
Department of Chemistry and Biochemistry
University of California
1156 High Street, Santa Cruz
CA 95064 (USA)

Supporting Information for this article can be found under http://dx.doi.org/10.1002/celc.201600178.

lytic activity.[10,11] Therefore, examples successfully illustrating this straightforward strategy are rare.

Hydrogen-bonded organic frameworks (HOFs), which are considered as intrinsically porous "polymers" with highly regular and tunable pores, have attracted extensive interest in many areas of research in, for example, selective gas adsorption, separation/purification and sensing.[12–15] Carbonization of HOFs is expected to result in highly porous carbon materials directly. In addition, contrary to the multiple steps involved in the synthesis of their two analogues, that is, metal–organic frameworks (MOFs) and covalent organic frameworks (COFs), HOFs can be easily prepared through the simple self-assembly of the building units in solution via intermolecular hydrogen bonding,[16–18] which are beneficial to the production scale up and cost reduction. However, to our knowledge, studies on the preparation of porous carbons derived from HOFs and their corresponding catalytic activity in the ORR are scarce.

In this study, by considering the high nitrogen content of melamine and its convenient assembly with trimesic acid to form a HOF in aqueous solution, we used a HOF comprising these two commercially available compounds as highly porous carbonaceous precursors to prepare mesoporous N-doped carbons. Carbonization of the HOF afforded a highly mesoporous carbon material with a nitrogen self-doped active site content of 4.8 atom% and a high surface area of 1321 $m^2 g^{-1}$. Electrochemical studies revealed that the obtained porous carbons showed ORR activity, and the best sample (HOF-800) exhibited a more efficient electrocatalytic activity for oxygen reduction as compared to the state-of-the-art Pt/C catalysts, in terms of onset potential, limiting current density, electron-transfer number, durability/stability, and tolerance to methanol crossover in alkaline media.

Experimental Section

Materials

Melamine and trimesic acid (98% purity) were purchased from Aladdin Industrial Inc (Shanghai, China). Pt/C (20% w/w) was purchased from Alfar Aesar.

Synthesis of HOF and HOF-T

In a typical synthesis, melamine (113.5 mg) and trimesic acid (189.1 mg) were separately dissolved in deionized water (150 mL) with stirring at 70 °C to form homogenous solutions (concentration 6 mM), and then an equal volume of both solutions were mixed together under stirring to initiate self-assembly. The resulting white precipitates were collected by centrifugation, washed thoroughly with deionized water, and then dried at 60 °C for 12 h in a vacuum oven. The dried precipitate (denoted HOF) was ground with $FeCl_3$ and the activation reagent $ZnCl_2$ at room temperature at a HOF/$FeCl_3$/$ZnCl_2$ mass ratio of 1:1:6 to form a homogeneous mixture, and then the mixture was thermally treated at controlled temperatures (700, 800 and 900 °C) for 2 h in a N_2 atmosphere with a gas flow rate of 300 sccm. After pyrolysis, the solids were soaked in aqueous HCl (1.0 M) for 8 h with ultrasonication, rinsed thoroughly with distilled water, and subsequently dried in a vacuum oven at about 65 °C overnight to obtain N-doped porous carbon HOF-*T* (*T* indicates the pyrolysis temperature). The whole process of the preparation of HOF-*T* is shown in Scheme 1.

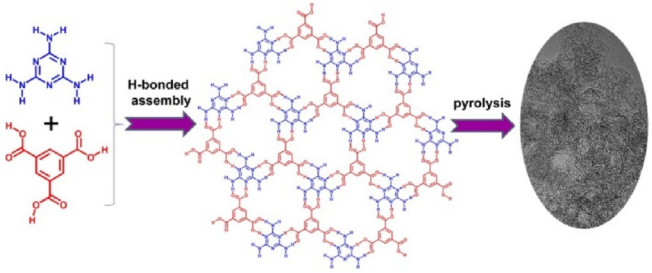

Scheme 1. The process of preparation of HOF-*T* porous carbons.

Characterization

Transmission electron microscopy (TEM) measurements were performed on a Tecnai G2-F20 electron microscope equipped with an EDX detector at an acceleration voltage of 100 kV. The samples for TEM measurements were prepared by drop-casting the catalyst dispersions directly onto copper grids precoated with a holey carbon film. Powder X-ray diffraction (XRD) characterization was conducted on a Bruker D8-Advance diffractometer using CuKα radiation. X-ray photoelectron spectroscopic (XPS) studies were performed with a Phi X-tool instrument.

The Brunauer–Emmett–Teller (BET) surface area was determined by using a Micromeritics ASAP 2010 analyzer measuring nitrogen adsorption at 77 K using the Barrett–Joyner–Halenda (BJH) method. Raman spectra were recorded on a Renishaw inVia instrument using an Ar laser source of 488 nm in a macroscopic configuration.

Electrochemical Measurements

Electrochemical measurements were performed on a CHI 750E electrochemical workstation (CH Instruments, Chenhua Co., Shanghai, China) in a conventional three-electrode cell, using a Pt wire as the counter electrode, an Ag/AgCl as the reference electrode, and a catalyst-modified glassy carbon electrode (GCE) as the working electrode. The catalysts inks were prepared by adding the catalyst into a solution containing isopropanol and Nafion (1%) at a volume ratio of 1:0.01 with ultrasonication to form a homogeneous suspension with a catalyst concentration of 0.999 mg mL^{-1}. A calculated amount (20 μL) of the suspension was then evenly cast onto the pre-cleaned GCE with a syringe and dried in air at room temperature; this amount corresponded to a catalyst loading of 101.9 μg cm^{-2}. Linear sweep voltammetry (LSV) was conducted in O_2-saturated KOH aqueous solution (0.1 M) with a catalyst-modified ring-disk electrode at various rotating speeds (100–2500 rpm).

2. Results and Discussion

Upon mixing aqueous solutions of melamine and trimesic acid, the 2D self-assembly of both molecules into HOFs was triggered, likely in a fashion shown in Scheme 1, and subsequently the 2D assemblies grew into 1D micrometer-scale rods (Figure 1a) through interplane π–π stacking.[17] Thermal treatment of these microrods at elevated temperature resulted in the carbonized HOF-*T* products. The graphitic D and G bands can be clearly observed in both HOF-700 and HOF-800 samples at ap-

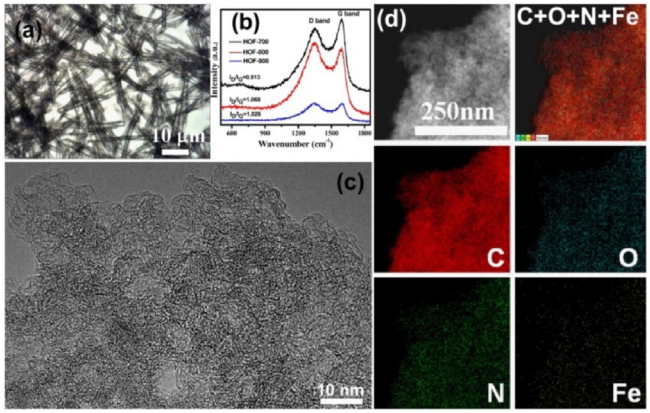

Figure 1. a) Optical microscopy image showing the morphology of HOFs. b) Raman spectra of HOF-*T* samples. c) Representative TEM image of HOF-800. d) TEM image of HOF-800 and corresponding elemental mapping images of C, O, N and Fe.

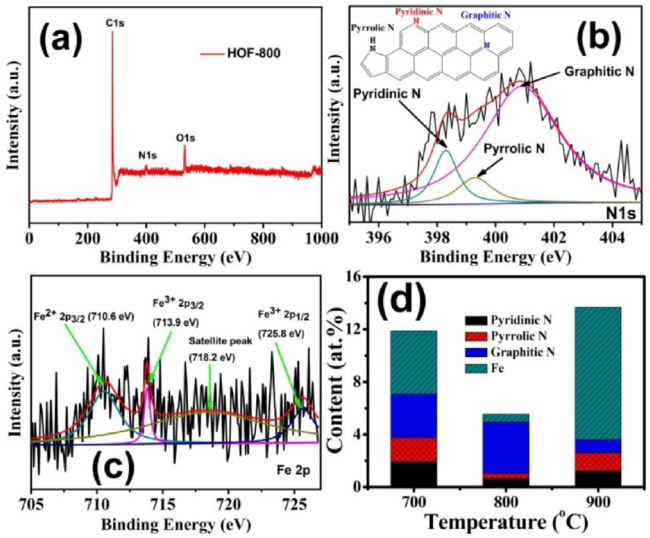

Figure 2. a) XPS survey spectra and corresponding high-resolution XPS scans of b) N 1s (inset: three N-doping configurations in graphene) and c) Fe 2p electrons for HOF-800. d) Concentrations of N dopants and Fe in HOF-*T* prepared at different temperatures.

proximately 1350 and 1590 cm^{-1}, respectively (Figure 1 b). Furthermore, the intensity ratio of the D and G bands (I_D/I_G) was 0.913 for HOF-700 and 1.068 for HOF-800, indicating a more disordered carbon skeleton in the latter, likely due to the introduction of more doping heteroatoms at an increased pyrolysis temperature from 700 to 800 °C.[3,19] A slightly decreased I_D/I_G ratio of 1.026 was observed for HOF-900, which might be due to the formation of more-graphitic carbons at this higher temperature.

A typical TEM image revealed the irregular sheet-like structure of HOF-800 (Figure 1 c). In addition, small wavy strips with a lattice spacing of approximately 0.36 nm (Figure S1 a in the Supporting Information) were found to homogeneously distributed within the sample, suggesting the formation of graphene nanosheets.[20,21] In the corresponding energy dispersive spectroscopy (EDS) mapping images (Figure 1 d), C, O, N, and Fe atoms were found to evenly distribute in HOF-800 with an apparent elemental content decreasing in the order of C > O ≈ N > Fe.

The elemental compositions in the HOF-800 were firstly analyzed by measuring XPS survey spectra. In Figure 2 a, the peaks assigned to the elements C, N, and O are well resolved (for the XPS spectra of HOF-700 and HOF-900 samples, see Figures S4 and S5). Based on the integrated peak areas, the total N content on the surface of HOF-800 was calculated to be 4.8 atom %. The N-bonding configurations (Figure 2 b) and Fe chemical states (Figure 2 c) on the surface of the carbon materials were investigated by high-resolution XPS measurements. As shown in Figure 2 b, the spectra of N 1s electrons can be deconvoluted into three peaks centered at 398.2, 399.4, and 401.0 eV, corresponding to pyridinic N, pyrrolic N and graphitic N, respectively. The presence of these three peaks indicated the successful incorporation of N dopants onto the carbon matrix[3,22–24] Notably, the total N content on the sample surface decreased from 6.2 atom % for HOF-700 to 4.8 atom % for HOF-800 and 3.6 atom % for HOF-900. In addition, the graphitic N became the dominant N dopants with a content increasing from 2.9 atom % for HOF-700 (Figure S4 b) to 3.7 atom % for HOF-800 (Figure 2 d), signifying the conversion of pyridinic N and pyrrolic N to more thermally stable graphitic N.[25–27] However, further increasing the pyrolysis temperature to 900 °C resulted in an abrupt decrease of graphitic N content to 1.0 atom % (Figure 2 d), likely due to the accompanying release of graphitic N with the removal of carbon matrix [see Eq. (5)]. Because the introduction of graphitic N into the carbon skeletons can enhance the conductivity of graphene sheets by facilitating electron transfer and hence promoting the ORR activity,[26,28] the high content of graphitic N in HOF-800 indicates a high catalytic activity of this material in the ORR.

In the high-resolution XPS spectrum of Fe 2p electrons (Figure 2 c), a weak signal was obtained due to the low concentration of Fe-containing species in HOF-800, which is supported by the EDS analysis (Figure S1 c). Nevertheless, several peaks could be assigned. The peak at 710.6 eV was derived from Fe^{2+}, whereas the two peaks at 713.9 and 725.8 eV originated from Fe^{3+}, with a satellite peak at 718.2 eV.[2,3] Based on the comparison of the integrated peak areas, the concentration of Fe was found to decrease from 4.8 atom % for the HOF-700 sample (Figure S4 c) to 0.6 atom % for HOF-800 (Figure 2 d), which is likely due to the evaporation of volatile $FeCl_3$ at high temperatures.[3,29] Further increasing the pyrolysis temperature to 900 °C led to a remarkable increase in Fe content to 10.1 atom % (Figure S5 c), along with a sharp increase in O content to 25.9 atom % and a sudden decrease in C content to 57.9 atom %, which indicates that the HOF-900 underwent pyrolysis through a different carbonization pathway as compared to HOF-700 and HOF-800. The atomic contents of related elements at different pyrolysis temperatures are summarized in Table 1.

XRD measurements were then conducted to determine the crystalline structures of HOF-*T* samples. As shown in Figure 3 a, a series of well-defined diffraction peaks at $2\theta = 18.36°$, 30.06°,

Table 1. Summary of the surface area, average pore size, and elemental content data of HOF-*T* samples.

Sample name	Surface area [$m^2 g^{-1}$]	Average pore size [nm]	C [atom %]	O [atom %]	Fe [atom %]	N [atom %]		
						Pyridinic N	Pyrrolic N	Graphitic N
HOF-700	926.85	2.60	76.0	9.9	4.8	1.666	1.625	2.909
HOF-800	1321	4.42	86.7	7.8	0.6	0.613	0.406	3.782
HOF-900	661.47	40.2	57.9	25.9	10.1	1.234	1.362	1.004

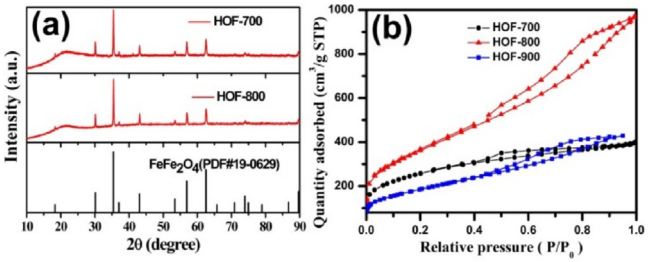

Figure 3. a) XRD patterns of HOF-700 and HOF-800. b) N_2 adsorption/desorption isotherms of the HOF-*T* samples.

35.44°, 37.10°, 43.12°, 53.44°, 57.04°, 62.56°, and 73.97° were observed for HOF-700 and HOF-800. These are consistent with the (111), (220), (311), (222), (400), (422), (511), (440), and (533) crystalline planes of Fe_3O_4 (JCPDS card no. 19-0629), respectively (Figure 3a). The presence of crystalline Fe_3O_4 even after acid etching signified that partial Fe_3O_4 nanoparticles in HOF-700 and HOF-800 were encapsulated by carbon. In addition, a broad diffraction peak centered at $2\theta = 21.68°$ was observed, corresponding to a d-spacing of 4.09 Å. This diffraction peak was attributed to the formation of graphitic carbon, which was consistent with the results observed by TEM (Figure S1). The XRD profile for HOF-900 (Figure S3) shows that the main Fe-containing compound within this sample was Fe_3C, which is consistent with the XPS results (Figure 2d), which demonstrate that the HOF-900 underwent a different carbonization mechanism compared to HOF-700 and HOF-800.

Taken together, the carbonization process of the HOF samples likely involves the following reactions [Eqs. (1)–(6)]:

$$ZnCl_2 + HOF \rightarrow ZnO + C_{N\text{-doped}} + H_2O\uparrow + HCl\uparrow + NH_3\uparrow + HCN\uparrow + CO_2\uparrow + CO\uparrow + H_2\uparrow \quad (1)$$

$$FeCl_3 + 3\,H_2O \rightarrow Fe(OH)_3 + 3\,HCl\uparrow \quad (2)$$

$$2\,Fe(OH)_3 \rightarrow Fe_2O_3 + 3\,H_2O\uparrow \quad (3)$$

$$6\,Fe_2O_3 + C \rightarrow 4\,Fe_3O_4 + CO_2\uparrow \quad (4)$$

$$Fe_3O_4 + 2\,C \rightarrow 3\,Fe + 2\,CO_2\uparrow \quad (5)$$

$$3\,Fe + C \rightarrow Fe_3C \quad (6)$$

Upon gradually heating a mixture comprising the HOF, $FeCl_3$ and $ZnCl_2$, the HOF was dehydrated and hence carbonized by the activation reagent $ZnCl_2$. In addition, $ZnCl_2$ was hydrolyzed into $Zn(OH)_2$, which was subsequently converted to ZnO, along with the formation of volatile HCl resulting from the $ZnCl_2$ hydrolysis. During the carbonization/degradation process of the HOF, a series of other volatile species such as water, hydrogen cyanide, ammonia, carbon dioxide, carbon monoxide, and hydrogen were released [Eq. (1)]. In the presence of water, $FeCl_3$ was firstly hydrolyzed into $Fe(OH)_3$ and then converted to Fe_2O_3, releasing the highly volatile hydrogen chloride [Eq. (2)] and water [Eq. (3)]. At relatively low pyrolysis temperatures ($\leq$800 °C), Fe_2O_3 reacted with carbon to form Fe_3O_4 and carbon dioxide [Eq. (4)]. However, at higher pyrolysis temperatures (>800 °C), Fe_3O_4 was fully reduced by carbon to form Fe^0 and CO_2 [Eq. (5)], leading to a sudden decrease of carbon content, as observed in the XPS measurements of HOF-900 (Figure 2d and Table 1). Simultaneously, the N dopants, especially the dominant graphitic N atoms, were largely released due to the removal of carbon matrix (Figure 2d and Table 1). At this high temperature, Fe^0 further reacted with carbon and finally formed Fe_3C in the product [Eq. (6)], which is consistent with the results from the XRD (Figure S3) and XPS (Figure 2d) measurements.

The specific surface area and pore structure of the above carbon materials were determined by BET measurements. Based on the N_2 adsorption/desorption isotherms of HOF-800 (Figure 3b), its specific surface area was determined to be 1321 $m^2 g^{-1}$, which is much higher than the value of 926.85 $m^2 g^{-1}$ determined for HOF-700 and 661.47 $m^2 g^{-1}$ for HOF-900. The average pore diameter of HOF-800 was calculated to be 4.42 nm, indicating the formation of mesopores. The high surface area as well as the mesoporous structure of HOF-800 are beneficial to the transfer of ORR-relevant species, and thus might promote the ORR catalytic activity.

Cyclic voltammetric measurements were performed in 0.1 M KOH solutions on a GCE to initially assess the ORR catalytic activity of HOF-*T* samples. In N_2-saturated electrolyte solution (Figure 4, black curves), all the porous carbons displayed a featureless double-layer charging curve between −0.04 and +1.16 V. On the basis of the integrated area of the double-layer charging profile, the electrochemical surface areas for all three porous carbons are in the order $S_{HOF-800} > S_{HOF-700} \gg S_{HOF-900}$, which is consistent with the results of the BET surface area measurements. In O_2-saturated electrolyte (red curves), a clear cathodic peak was observed at +0.811 V for HOF-700, +0.844 V for HOF-800 and +0.556 V for HOF-900, indicative of the apparent ORR catalytic activity for the porous carbons. Note that, the oxygen reduction peak for the HOF-800 catalyst appeared at almost the same potential position as that of

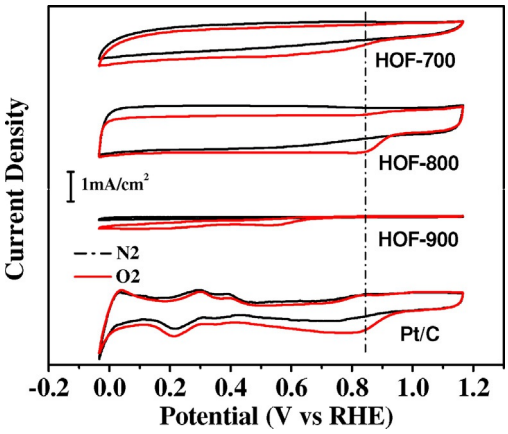

Figure 4. CV curves of HOF-*T* samples and Pt/C in N_2-saturated (black dashed–dotted line) and O_2-saturated (red solid line) 0.1 M KOH solution at a potential sweep rate of 50 mV s^{-1}.

a commercial Pt/C catalyst. More significantly, the peak current of the HOF-800 (1.167 mA cm^{-2}) was markedly higher than those of the HOF-700 (0.667 mA cm^{-2}) and HOF-900 (0.278 mA cm^{-2}). These results signified that the HOF-800 was the best catalyst among the HOF-*T* series.

In the rotating disk electrode (RDE) voltammograms (Figure 5a), nonzero cathodic current was observed at +0.930 V (vs. RHE) in the HOF-700 sample when the electrode potential was scanned negatively between +1.166 and −0.033 V. For HOF-800, the onset potential was observed at the much more positive value of +0.962 V; in sharp contrast, for HOF-900, it was severely reduced to +0.669 V. Moreover, the limiting currents of HOF-*T* samples were found to be highly dependent on the pyrolysis temperature. For example, the diffusion-limited currents at +0.400 V were 3.10 mA cm^{-2} for HOF-700, 4.19 mA cm^{-2} for HOF-800, and 1.20 mA cm^{-2} for HOF-900, which suggested that the HOF-800 sample outperformed the other two catalysts in the ORR. Notably, HOF-800 showed a higher concentration of graphitic N and larger surface area compared to HOF-700 and HOF-900 (Table 1), indicating that graphitic N likely played a critical role in determining the ORR activity of these HOF-*T* samples.

Consistent results were obtained in the rotating ring-disk electrode (RRDE) voltammetric measurements. As shown in Figure 5b, the onset potential was identified at +0.929 V for Pt/C (dashed black curve) from its corresponding linear polarization curve, whereas the more positive onset potential of +0.962 V was observed for HOF-800 (solid red curve), indicating that a lower overpotential was needed to catalyze the ORR on HOF-800. In addition, the limiting current of HOF-800 was higher than that for Pt/C, that is, 4.19 mA cm^{-2} for HOF-800 compared to 3.99 mA cm^{-2} for Pt/C at +0.40 V, again suggesting a higher catalytic activity of HOF-800 than Pt/C.

The number of electrons transferred *n* and peroxide yield from the ORR involving the carbon materials were calculated by using Equations (7) and (8), respectively:

$$n = \frac{4i_d}{i_r/N + i_d} \tag{7}$$

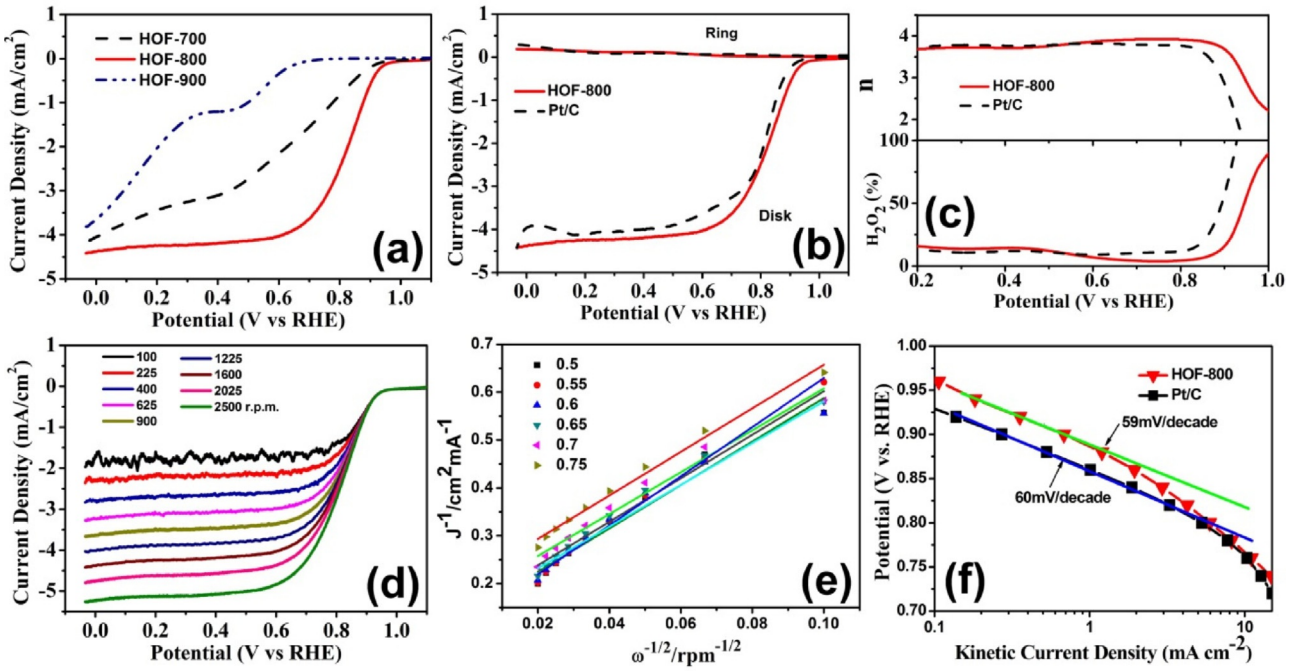

Figure 5. a) RDE voltammograms of HOF-*T* samples. b) RRDE voltammograms and c) the plots of H_2O_2 yield and number of transferred electrons *n* of GCEs modified with HOF-800 and Pt/C catalysts at a rotation speed of 1600 rpm. d) LSV curves for HOF-800 at various rotating speeds, and e) the corresponding K–L plots at the potentials indicated. f) Tafel plots of HOF-800 and Pt/C catalysts. All measurements were performed with a catalyst loading of 101.9 μg cm^{-2} in an O_2-saturated 0.1 M KOH aqueous solution at a sweep rate of 10 mV s^{-1}.

$$\%HO_2^- = 200 \times \frac{i_r/N}{i_r/N + i_d} \quad (8)$$

where the collection efficiency of the Pt ring electrode N was determined to be 37%[30–32] according to the reduction of 10 mM K_3[Fe(CN)6] in 0.1 M KCl[1] (Figure S8), and i_r and i_d are the voltammetric currents at the ring and disk electrodes, respectively. As shown in Figure 5c, the average n value for HOF-800 was calculated to be approximately 3.87, slightly higher than that of commercial Pt/C ($n = 3.80$). The corresponding H_2O_2 yield was estimated to be less than 12.5% for HOF-800 in the low overpotential region (+0.50–+0.80 V). Figure 5d shows the RRDE voltammograms of the HOF-800-modified electrode, from which it is apparent that the limiting currents steadily increased with increasing rotation speed. In the corresponding Koutecky–Levich (K–L) plots (Figure 5e), linear fits with an almost constant slope were made between 0.50 and +0.75 V, suggesting first-order ORR kinetics that are proportional to the O_2 concentration in solution. From the corresponding Tafel plots (Figure 5f), highly comparable slopes were measured for HOF-800 (59 mV dec^{-1}) and Pt/C (60 mV dec^{-1}), indicating that the rate-determining step for ORR at both catalysts was likely the first electron reduction of oxygen.[33–35]

Moreover, electrochemical impedance studies (Figure S6) revealed that the charge-transfer resistance of HOF-800 was much lower than that of other HOF-*T* samples in this study, and even lower than that of commercial Pt/C, consistent with the superior ORR activity of HOF-800. Notably, HOF-800 also showed lower intrinsic resistance than HOF-700 and HOF-900. This suggests that the inclusion of more graphitic N dopants onto graphene planes likely reduced the electrical resistance of the catalyst, which helped to improve the ORR activity.

As demonstrated above, the HOF-800, which was co-doped with N and Fe, showed high ORR activity in alkaline solution. One question immediately arises—what are the active sites for the ORR in HOF-800? In the literature, two mechanisms have been generally proposed to explain the emergence of ORR catalytic activity in Fe–N/C catalysts. One mechanism relies on the formation of highly active Fe–N_x moieties,[36,37] and the other involves the breakdown of electron neutrality along the graphene surface due to the inclusion of N dopants in the carbon matrix.[38,39] To shed light on the above question, a series of experiments to probe the active sites were further conducted. As reported in literature, thiocyanate ions (SCN^-) can form strong coordination bonds with Fe-containing species and hence efficiently block the corresponding Fe-containing sites. Therefore, if Fe-containing compounds serve as the actual active sites for the ORR in our HOF-*T* samples, the catalytic activity should decrease after treatment with an aqueous thiocyanate solution.[37] In the control experiments, electrochemical tests were performed on a HOF-800-modified GCE in an O_2-saturated 0.1 M KOH aqueous solution in the presence (red dashed curve) and absence (black solid curve) of 10 mM KSCN. As revealed in the RDE voltammogram (Figure 6a), the addition of KSCN to the electrolyte solution caused an apparent negative shift of 65 mV in the half-wave potential as well as an approximate 30% decrease of the limiting currents. These observations unambiguously verified that Fe-containing species were actually involved in the ORR, which is consistent with recent reports in the literature that the Fe–N_x moieties in Fe–N/C catalyst are active sites,[40,41] but that their contributions to the overall ORR activity are small. Although the actual active Fe species in our HOF-800 catalyst were not identified because of their very low concentration, both the chemically stable and labile forms, such as Fe–N_x compounds and Fe_3O_4 nanoparticles, were possibly involved in the ORR, as indicated by the XPS results (Figure 2).[1,3,42,43] Because the HOF-800 can retain more than 60% of its original ORR current after thiocyanate poisoning, it is reasonable to conclude that the Fe-free active sites consisting of N dopants mainly contributed to the ORR activity. Various recent studies in the literature suggest that the incorporation of graphitic N dopants into carbon skeletons causes substantial reduction of electron density on adjacent carbon atoms due to the stronger electronegativity of N compared to C, hence partial electrons are transferred from adjacent C atoms to the N dopants, and simultaneously the lone electron pairs on N atoms back-donate partial electrons to the adjacent C p_z orbitals through n–π conjugation.[44,45] These electron interactions between graphitic N dopants and adjacent C nuclei not only promote the formation of a transition chemical bond between O and C that favors O_2 adsorption, but also help to dissociate the O–O bond,[44] which are two important steps of the ORR. Thus, graphitic N is considered to promote ORR.[2]

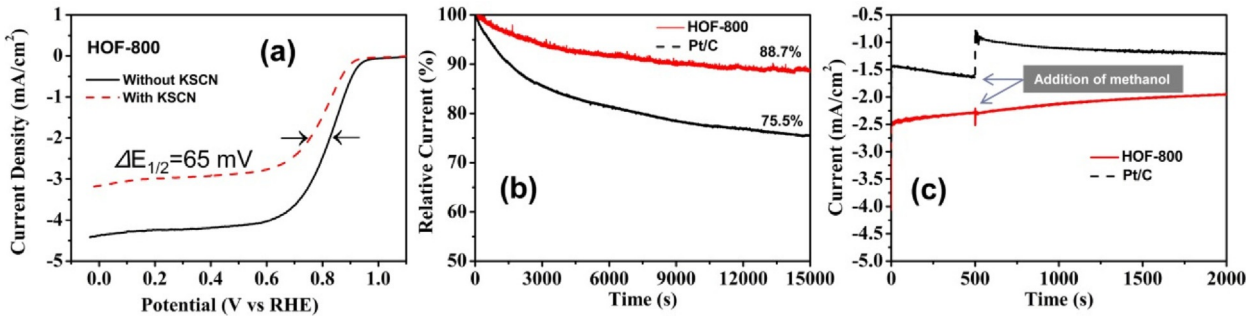

Figure 6. a) LSV curves of HOF-800 in the presence (red dashed curve) and absence of 10 mM KSCN (black solid curve). b) Chronoamperometric curves of HOF-800 and Pt/C at +0.70 V vs. RHE. c) The chronoamperometric curves of HOF-800 and Pt/C at +0.70 V before and after the addition of methanol (1 M). All measurements were conducted in an O_2-saturated 0.1 M KOH aqueous solution with an electrode rotation speed of 900 rpm.

Furthermore, the mesoporous structure of present carbons has been proposed to enhance the transfer of reaction intermediates and products. Taken together, the above results indicate that the efficient ORR activity of HOF-800 can be ascribed to both the Fe and graphitic N dopants along with the formation of mesopores.

Long durability was highly desired for these catalysts. The durability of the HOF-800 and commercial Pt/C catalysts for ORR was studied by chronoamperometric measurements. As shown in Figure 6b, after continuous working for 15000 s, the Pt/C electrode retained only 75.5% of the initial voltammetric current, whereas the HOF-800 catalyst retained a much higher voltammetric current of 88.7% under the same testing conditions, indicating better durability of HOF-800 than Pt/C in the ORR. Furthermore, the tolerance against methanol crossover is another concern of ORR catalysts. For the commercial Pt/C electrode (Figure 6c, black dashed curve), the addition of 1 M methanol into the electrolyte solution caused a sudden decrease of the voltammetric current due to methanol oxidation on the surface of this electrode. Although the voltammetric current slowly recovered to the negative side (ORR), even after 1500 s it only recovered to half of its initial value. However, only a slight decrease of the ORR current was observed at the HOF-800 electrode (Figure 6c, solid red curve), suggesting stronger tolerance to methanol crossover of HOF-800 compared to commercial Pt/C catalysts.

Additional control experiments were conducted by using melamine as the sole C and N sources. However, no carbon catalyst was obtained, probably because melamine completely sublimated or degraded during high-temperature pyrolysis. This result showed the necessity of trimesic acid in the preparation of porous carbon materials in this study.

Considering the availability of an abundance of HOFs with highly tunable chemical structures, there is much scope for further improving the ORR activity of HOF-derived carbons by careful choice of the assembly components, controlling the pore structures, and optimizing the pyrolysis conditions.

3. Conclusions

In conclusion, mesoporous N-doped carbons with high surface area were prepared by direct pyrolysis of an intrinsic porous HOF precursor, which could be conveniently obtained by self-assembly of the inexpensive, commercially available melamine and trimesic acid in aqueous solutions. Electrochemical measurements demonstrated that the HOF-800 sample had the best ORR activity among the series, with an overall catalytic performance even better than the commercial Pt/C catalysts in terms of production cost, onset potential, electron-transfer numbers, durability and resistance to the methanol crossover. Active-site-probing experiments suggested that the ORR activity of HOF-800 can be primarily attributed to the graphitic N dopants, along with partial contributions by the Fe-containing species that derived from the $FeCl_3$ used for activation. The results presented herein might encourage the utilization of highly porous HOFs for the preparation and engineering of carbon nanocomposites for efficient and cost-effective catalysts for oxygen reduction.

Acknowledgements

This work was supported by the National Natural Science Foundation of China (NSFC 51402111) and the Fundamental Research Funds for the Central Universities (SCUT Grant No. 2153860). S.W.C. thanks the National Natural Science Foundation of China (NSFC 21528301) for partial financial support.

Keywords: electrocatalysts · hydrogen-bonded organic frameworks · nitrogen doping · oxygen reduction reaction · porous carbon

[1] G. Wu, K. L. More, C. M. Johnston, P. Zelenay, *Science* **2011**, *332*, 443–447.
[2] L. Lin, Q. Zhu, A.-W. Xu, *J. Am. Chem. Soc.* **2014**, *136*, 11027–11033.
[3] W. Niu, L. Li, X. Liu, N. Wang, J. Liu, W. Zhou, Z. Tang, S. Chen, *J. Am. Chem. Soc.* **2015**, *137*, 5555–5562.
[4] Y.-C. Wang, Y.-J. Lai, L. Song, Z.-Y. Zhou, J.-G. Liu, Q. Wang, X.-D. Yang, C. Chen, W. Shi, Y.-P. Ren, M. Rauf, S.-G. Sun, *Angew. Chem. Int. Ed.* **2015**, *54*, 9907–9910; *Angew. Chem.* **2015**, *127*, 10045–10048.
[5] B. Men, Y. Sun, M. Li, C. Hu, M. Zhang, L. Wang, Y. Tang, Y. Chen, P. Wan, J. Pan, *ACS Appl. Mater. Interfaces* **2016**, *8*, 1415–1423.
[6] H.-W. Liang, W. Wei, Z.-S. Wu, X. Feng, K. Müllen, *J. Am. Chem. Soc.* **2013**, *135*, 16002–16005.
[7] Z. Wu, Y. Lv, Y. Xia, P. A. Webley, D. Zhao, *J. Am. Chem. Soc.* **2012**, *134*, 2236–2245.
[8] R. Silva, D. Voiry, M. Chhowalla, T. Asefa, *J. Am. Chem. Soc.* **2013**, *135*, 7823–7826.
[9] C. Liang, Z. Li, S. Dai, *Angew. Chem. Int. Ed.* **2008**, *47*, 3696–3717; *Angew. Chem.* **2008**, *120*, 3754–3776.
[10] Y. She, Z. Lu, M. Ni, L. Li, M. K. H. Leung, *ACS Appl. Mater. Interfaces* **2015**, *7*, 7214–7221.
[11] H. Zhu, J. Yin, X. Wang, H. Wang, X. Yang, *Adv. Funct. Mater.* **2013**, *23*, 1305–1312.
[12] Z. Sun, Y. Li, L. Chen, X. Jing, Z. Xie, *Cryst. Growth Des.* **2015**, *15*, 542–545.
[13] P. Li, Y. He, Y. Zhao, L. Weng, H. Wang, R. Krishna, H. Wu, W. Zhou, M. O'Keeffe, Y. Han, B. Chen, *Angew. Chem. Int. Ed.* **2015**, *54*, 574–577; *Angew. Chem.* **2015**, *127*, 584–587.
[14] P. Li, Y. He, H. D. Arman, R. Krishna, H. Wang, L. Weng, B. Chen, *Chem. Commun.* **2014**, *50*, 13081–13084.
[15] X.-Z. Luo, X.-J. Jia, J.-H. Deng, J.-L. Zhong, H.-J. Liu, K.-J. Wang, D.-C. Zhong, *J. Am. Chem. Soc.* **2013**, *135*, 11684–11687.
[16] Y.-S. Jun, E. Z. Lee, X. Wang, W. H. Hong, G. D. Stucky, A. Thomas, *Adv. Funct. Mater.* **2013**, *23*, 3661–3667.
[17] H. Wang, X. Xu, N. M. Johnson, N. K. R. Dandala, H.-F. Ji, *Angew. Chem. Int. Ed.* **2011**, *50*, 12538–12541; *Angew. Chem.* **2011**, *123*, 12746–12749.
[18] H.-F. Ji, X. Xu, *Langmuir* **2010**, *26*, 4620–4622.
[19] F. J. Maldonado-Hódar, C. Moreno-Castilla, J. Rivera-Utrilla, Y. Hanzawa, Y. Yamada, *Langmuir* **2000**, *16*, 4367–4373.
[20] X. Liu, L. Li, W. Zhou, Y. Zhou, W. Niu, S. Chen, *ChemElectroChem.* **2015**, *2*, 803–810.
[21] S. Zhuang, X. Xu, B. Feng, J. Hu, Y. Pang, G. Zhou, L. Tong, Y. Zhou, *ACS Appl. Mater. Interfaces* **2014**, *6*, 613–621.
[22] Z.-H. Sheng, L. Shao, J.-J. Chen, W.-J. Bao, F.-B. Wang, X.-H. Xia, *ACS Nano* **2011**, *5*, 4350–4358.
[23] L. Qu, Y. Liu, J.-B. Baek, L. Dai, *ACS Nano* **2010**, *4*, 1321–1326.
[24] P. Chen, L.-K. Wang, G. Wang, M.-R. Gao, J. Ge, W.-J. Yuan, Y.-H. Shen, A.-J. Xie, S.-H. Yu, *Energy Environ. Sci.* **2014**, *7*, 4095–4103.
[25] L. Lai, J. R. Potts, D. Zhan, L. Wang, C. K. Poh, C. Tang, H. Gong, Z. Shen, J. Linc, R. S. Ruoff, *Energy Environ. Sci.* **2012**, *5*, 7936–7942.
[26] H.-S. Oh, J.-G. Oh, B. Roh, I. Hwang, H. Kim, *Electrochem. Commun.* **2013**, *13*, 879–881.

[27] T. Sharifi, G. Hu, X. Jia, T. Wågberg, *ACS Nano* **2012**, *6*, 8904 – 8912.
[28] Z. Yang, H. Nie, X. Chen, X. Chen, S. Huang, *J. Power Sources* **2013**, *236*, 238 – 249.
[29] W. Niu, L. Li, J. Liu, N. Wang, W. Li, Z. Tang, W. Zhou, S. Chen, *Small* **2016**, *12*, 1900 – 1908.
[30] Y. Yao, H. Xiao, P. Wang, P. Su, Z. Shao, Q. Yang, *J. Mater. Chem. A* **2014**, *2*, 11768 – 11775.
[31] R. Zhang, S. He, Y. Lu, W. Chen, *J. Mater. Chem. A* **2015**, *3*, 3559 – 3567.
[32] J. Sanetuntikul, C. Chuaicham, Y.-W. Choi, S. Shanmugam, *J. Mater. Chem. A* **2015**, *3*, 15473 – 15481.
[33] M. H. Robson, A. Serov, K. Artyushkova, P. Atanassov, *Electrochim. Acta* **2013**, *90*, 656 – 665.
[34] N. Wang, W. Niu, L. Li, J. Liu, Z. Tang, W. Zhou, S. Chen, *Chem. Commun.* **2015**, *51*, 10620 – 10623.
[35] J. Xu, P. Gao, T. S. Zhao, *Energy Environ. Sci.* **2012**, *5*, 5333 – 5339.
[36] M. Lefèvre, J. P. Dodelet, P. Bertrand, *J. Phys. Chem. B* **2002**, *106*, 8705 – 8713.
[37] Q. Wang, Z.-Y. Zhou, Y.-J. Lai, Y. You, J.-G. Liu, X.-L. Wu, E. Terefe, C. Chen, L. Song, M. Rauf, N. Tian, S.-G. Sun, *J. Am. Chem. Soc.* **2014**, *136*, 10882 – 10885.
[38] K. Gong, F. Du, Z. Xia, M. Durstock, L. Dai, *Science* **2009**, *323*, 760 – 764.
[39] N. Daems, X. Sheng, I. F. J. Vankelecom, P. P. Pescarmona, *J. Mater. Chem. A* **2014**, *2*, 4085 – 4110.
[40] M.-Q. Wang, W.-H. Yang, H.-H. Wang, C. Chen, Z.-Y. Zhou, S.-G. Sun, *ACS Catal.* **2014**, *4*, 3928 – 3936.
[41] J. Liu, X. Sun, P. Song, Y. Zhang, W. Xing, W. Xu, *Adv. Mater.* **2013**, *25*, 6879 – 6883.
[42] C. He, J. J. Zhang, P. K. Shen, *J. Mater. Chem. A* **2014**, *2*, 3231 – 3236.
[43] D. Huang, Y. Luo, S. Li, M. Wang, Y. Shen, *Electrochim. Acta* **2015**, *174*, 933 – 939.
[44] D. Deng, X. Pan, L. Yu, Y. Cui, Y. Jiang, J. Qi, W.-X. Li, Q. Fu, X. Ma, Q. Xue, G. Sun, X. Bao, *Chem. Mater.* **2011**, *23*, 1188 – 1193.
[45] H. Kim, K. Lee, S. I. Woo, Y. Jung, *Phys. Chem. Chem. Phys.* **2011**, *13*, 17505 – 17510.

Manuscript received: April 5, 2016
Accepted Article published: April 28, 2016
Final Article published: May 17, 2016